

1 Metamorphism during temperature gradient with undersaturated advective
2 airflow in a snow sample

3
4 Pirmin Philipp Ebner^{1,2}, Martin Schneebeli^{2,*}, and Aldo Steinfeld¹

5 ¹ *Department of Mechanical and Process Engineering, ETH Zurich, 8092 Zurich, Switzerland*

6 ² *WSL Institute for Snow and Avalanche Research SLF, 7260 Davos-Dorf, Switzerland*

7
8
9 **Abstract**

10 Snow at or close to the surface commonly undergoes temperature gradient meta-
11 morphism under advective flow, which alters its microstructure and physical properties.
12 Time-lapse X-ray micro-tomography is applied to investigate the structural dynamics of
13 temperature gradient snow metamorphism exposed to an advective airflow in controlled
14 laboratory conditions. Cold saturated air at the inlet was blown into the snow samples
15 and warmed up while flowing across the sample with a temperature gradient of around
16 50 K m⁻¹. Changes of the porous ice structure were observed at mid-height of the snow
17 sample. Sublimation occurred due to the slight undersaturation of the incoming air into
18 the warmer ice matrix. Diffusion of water vapor opposite to the direction of the temper-
19 ature gradient counteracted the mass transport of advection. Therefore, the total net ice
20 change was negligible leading to a constant porosity profile. However, the strong re-
21 crystallization of water molecules in snow may impact its isotopic or chemical content.

22 *Keywords:* snow, temperature gradient, metamorphism, advection, sublimation, tomography

* Corresponding author. Email: schneebeli@slf.ch.

24 **1. Introduction**

25 Snow has a complex porous microstructure and consists of a continuous ice struc-
26 ture made of grains connected by bonds and inter-connecting pores (Löwe et al., 2011).
27 It has a high permeability (Calonne et al, 2012, Zermatten et al., 2014) and under ap-
28 propriate conditions airflow through the snow structure can occur (Sturm and Johnson,
29 1991) due to variation of surface pressure (Colbeck, 1989; Albert and Hardy, 1995),
30 simultaneous warming and cooling, and induced temperature gradients (Sturm and
31 Johnson, 1991). Both diffusive and advective airflows affect heat and mass transport in
32 the snowpack and influence chemical concentrations (Gjessing, 1977; Waddington et
33 al., 1996). Various airflow conditions in a snow sample occur, namely: isothermal air-
34 flow, air cooling by a negative temperature gradient along the airflow leading to a local
35 supersaturation of the air, and air warming by a positive temperature gradient along the
36 airflow leading to a local undersaturation of the air (Fig. 1). In general, in a natural
37 snowpack close to the surface ($< 1\text{cm}$) two additional conditions can occur: (1) warm air
38 enters a snowpack having a positive temperature gradient leading to a supersaturation of
39 the air at the entrance, and (2) cold air enters a snowpack having a negative temperature
40 gradient leading to an undersaturation of the air at the entrance. However, because snow
41 has a high heat capacity compared to the air, a high specific surface area, and therefore a
42 high convective heat transfer to the air, a “quasi” thermal equilibrium (the term “quasi”
43 is used because normally the snow structure continuously changes and therefore the
44 equilibrium conditions as well) is usually assumed inside the snowpack ($> 1\text{ cm}$). In this
45 paper, only conditions deeper than $> 1\text{ cm}$ inside a snowpack are considered. Under iso-
46 thermal condition, the continuous sublimation and deposition of ice is due to higher va-
47 por pressure over convex surfaces and lower vapor pressure over concave surfaces, re-
48 spectively (Kelvin-effect) (Neumann et al., 2008; Ebner et al., 2014). However, apply-
49 ing a fully isothermal saturated airflow across a snow sample has been shown to have
50 no influence on the coarsening rate that is typical for isothermal snow metamorphism
51 independently of the transport regime in the pores at a physically possible Peclet-
52 number (Ebner et al., 2015a). When applying a temperature gradient, the effect of sub-
53 limation and deposition in the snow results from interaction between snow temperature
54 and the local relative humidity in the pores. If vapor is advected from a warmer zone
55 into a colder zone, the air becomes supersaturated, and some water vapor deposits onto
56 the surrounding ice grains. This leads to a change in the microstructure creating whisk-

57 er-like crystals (Ebner et al., 2015b). Whisker-like crystals are very small ($\sim 10\text{-}30\ \mu\text{m}$)
58 elongated monocrystals. A flow rate dependence of the deposition rate of water vapor
59 deposition at the ice interface was observed, asymptotically approaching an average es-
60 timated maximum volumetric deposition rate on the whole sample of $1.05 \cdot 10^{-4}\ \text{kg m}^{-3}$
61 s^{-1} (Ebner et al., 2015b). Contrarily, if the temperature gradient acts in the same direc-
62 tion of the airflow, the airflow through the snow brings cold and relatively dry air into a
63 warmer area, causing that the pore space air becomes undersaturated, and surrounding
64 ice sublimates. Here, we investigate specifically this last effect.

65 Sublimation of snow is a fundamental process that affects its crystal structure
66 (Sturm and Benson, 1997), and thus is important for ice core interpretation (Stichler et
67 al., 2001; Ekaykin et al., 2009), as well as calculation of surface energy balance (Box
68 and Steffen, 2001) and mass balance (Déry and Yau, 2002). Kaempfer and Plapp (2009)
69 suggest that condensation of water vapor will have a noticeable effect on the micro-
70 structure of snow using a 3D phase-field model, which is also confirmed by a two di-
71 mensional finite-element model using airflow velocities, vapor transport and sublima-
72 tion rates of Albert (2002). Neumann et al. (2009) determined that there is no energy
73 barrier to be overcome during sublimation, and suggest that snow sublimation is limited
74 by vapor diffusion into pore space, rather than by sublimation at the crystal surface.

75 In the present work, we studied the surface dynamics of snow metamorphism under
76 an induced temperature gradient and saturated airflow in a controlled laboratory exper-
77 iments. Cold saturated air at around $-14\ \text{°C}$ was blown into the snow samples and
78 warmed up to around $-12.5\ \text{°C}$ while flowing across the sample. Sublimation of ice was
79 analyzed by in-situ time-lapse experiment with microcomputer tomography (micro-CT)
80 (Pinzer and Schneebeli, 2009; Chen and Baker, 2010; Pinzer et al., 2012; Wang and
81 Baker, 2014; Ebner et al., 2014) to obtain the discrete-scale geometry of snow. By using
82 discrete-scale geometry, all structures are resolved with a finite resolution correspond-
83 ing to the voxel size.

84 **2. Time-Lapse tomography experiments**

85 Temperature gradient experiments with fully saturated airflow across snow samples
86 (Ebner et al., 2014) were performed in a cooled micro-CT (Scanco Medical $\mu\text{-CT}80$) in
87 a cold laboratory temperature of $T_{\text{lab}} = -15\ \text{°C}$. Cold saturated air was blown into the
88 snow samples and warmed up while flowing across the sample. Aluminum foam includ-
89 ing a heating wire was used to warm the side of the snow opposite to the entering air-

90 flow. We analyzed the following flow rates: a volume flow of 0 (no advection), 0.3, 1.0,
91 and 3.0 liter/min. Higher flow rates were experimentally not possible as shear stresses
92 by airflow destroyed the snow structure (Ebner et al., 2015a). Nature identical snow
93 produced in a cold laboratory (Schleef et al., 2014) was used for the snow sample prepa-
94 ration (water temperature: 30 °C; air temperature: -20 °C). The snow was sieved with a
95 mesh size of 1.4 mm into a box, and was sintered for 27 days at -5°C to increase its
96 strength. The sample holder (diameter: 53 mm; height: 30 mm) was filled by cutting out
97 a cylinder from the sintered snow and pushing into the sample holder without mechani-
98 cal disturbance of the core. The snow samples were measured with a voxel size of 18
99 μm^3 over 108 h with time-lapse micro-CT measurements taken every 3 h, producing a
100 sequence of 37 images. The size of the cubic voxel size was 18 μm^3 . The innermost 36.9
101 mm of the total 53 mm diameter were scanned, and subsamples with a dimension of 7.2
102 mm \times 7.2 mm \times 7.2 mm were extracted for further processing. The imaged volume was
103 in the centre of the sample (Fig. 1 c)). A linear encoder with a resolution of less than 1
104 voxel ($< 2 \mu\text{m}$) was used to verify that the scans were taken at the same position. The
105 reconstructed micro-CT images were filtered by using a $3 \times 3 \times 3$ median filter followed
106 by a Gaussian filter ($\sigma = 1.4$, support = 3). The clustering-based Otsu method (Otsu,
107 1979) was used to automatically segment the grey-level images into ice and void phase.
108 Morphological properties of the two-phase system were determined based on the geom-
109 etry obtained by the micro-CT. The segmented data were used to calculate a triangulat-
110 ed ice matrix surface and tetrahedrons inscribed into the ice structure. Morphological
111 parameters such as porosity (ε) and specific surface area (SSA) were then calculated. An
112 opening-based morphological operation was applied to extract the mean pore size of
113 each micro-CT scan (d_{mean}) (Haussener et al., 2012). As additional physical and struc-
114 tural parameter, the effective thermal conductivity k_{cond} was estimated by direct pore-
115 level simulations (DPLS) to determine the influence of changing microstructure. DPLS
116 determined the effective thermal conductivity by solving the governing steady-state heat
117 conduction equations within the solid phase and the stagnant fluid phase (Kaempfer et
118 al., 2005; Petrasch et al., 2008; Calonne et al., 2011; Löwe et al., 2013).

119

120 **3. Results**

121 Time-lapse tomographic scans were performed with temperature gradients between
122 43-53 K m^{-1} (Table 1). Small fluctuations of the measured inlet and outlet temperature

123 were due to temperature regulation both inside the cold chamber and inside the micro-
124 CT (Ebner et al., 2014). A shift of $\Delta t < 10$ min between inlet and outlet temperature in-
125 dicated that a fast equilibrium between the temperature of the snow and the airflow was
126 reached (Albert and Hardy, 1995; Ebner et al., 2015b). The morphological evolution
127 was similar between all four experiments and only a slight rounding and coarsening was
128 visually observed, shown in Fig. 2. The initial ice grains did not change with time and
129 the locations of sublimation and deposition for “ota3” and “ota4” is shown in Fig. 3.
130 Sublimation of 7.7 % and 7.6 % of the ice matrix and deposition of 6.0 % and 9.6 % on
131 the ice matrix were observed. The data were extracted by superposition of vertical
132 cross-sections at 0 and 108 hours with an uncertainty of 6%. The mass sublimated pref-
133 erentially at locations of the ice matrix with low radii and was relocated leading to a
134 smoothing of the ice surface and to an increase in the size of pores (Fig. 4 a)). The pore
135 size (uncertainty ~ 6 %) increased by 3.4 %, 3.6 %, 5.4 % and 6.5 % for ‘ota1’, ‘ota2’,
136 ‘ota3’, and ‘ota4’, respectively.

137 Loss of ice due to sublimation could not be detected by the micro-CT scans due to
138 limited accuracy and no flow rate dependence was observed during any of the four ex-
139 periments. The temporal evolution of the porosity, shown in Fig. 4 b), did not change
140 with time and the influence of sublimation of water vapor was not observed. Only ‘ota2’
141 showed a slight drop in the temporal evolution of the porosity until 18 h into the exper-
142 iment but kept constant afterwards. This slight drop (≈ 0.5 %) was probably caused by
143 settling of the snow. Coarsening was observed for each experiment but the influence of
144 changing airflow was not visible, confirmed by the temporal SSA evolution, shown in
145 Fig. 4 c).

146 The repositioning of water molecules led to a smoothing of the ice grains, but did
147 not affect the thermal conductivity of snow. This quantity (standard deviation ~ 0.025 W
148 m^{-1}) slightly increased after applying airflow to the temperature gradient, shown in Fig.
149 4 d), but no flow rate dependence was observed. Every third scan was used to extract
150 the thermal conductivity and a change of -2.6 %, 3.6 %, 2.2 %, and 2.7 % for ‘ota1’,
151 ‘ota2’, ‘ota3’, and ‘ota4’ was detected.

152

153 **5. Discussion**

154 The rate of deposition onto the ice surface depends on the flow rate where warm
155 saturated air cooled down while flowing through the sample, as shown in previous ex-

156 periments (Ebner et al., 2015b). Its deposition rate asymptotically reached a maximum
157 of $1.05 \cdot 10^{-4} \text{ kg m}^{-3} \text{ s}^{-1}$. In this study, changing the temperature gradient leads to a
158 warming up of a cold saturated flow, and resulted in a sublimation rate too small for the
159 analyzed period of the experiment to measure a flow rate dependence by the micro-CT
160 and an influence on the temporal density gradient. A smoothing of ice grains and an in-
161 crease of the pore space was measured but the airflow velocity did not affect the reloca-
162 tion process of water molecules.

163 A structural change of the ice grains and repositions of water molecules was ob-
164 served but the total net flux of the snow was not affected. The superposition of a vertical
165 cross-section in Fig. 3 shows a big effect on reposition of water molecules on the ice
166 structure. However, the temporal porosity (Fig. 4 b) was not affected and the total water
167 vapor net flux was negligible for the analyzed volume. Continued sublimation and dep-
168 osition of water molecules due the temperature gradient led to a saturation of the pore
169 space. The vapour pressure of the air in the pore was in equilibrium with the water pres-
170 sure of the ice, given by the local temperature. The entering air warmed up, allowing
171 vapour sublimating from the snow sample to be incorporated into the airflow. As time
172 passed, the snow grains in the sample became more rounded as convexities sublimated.
173 As a result of the reduced curvature, the rate of sublimation decreased and less vapour
174 was deposited in concavities and therefore the surface asperities persisted longer. Final-
175 ly, the “Kelvin-effect” had a longer impact on the structural change of the ice grains and
176 the reposition of water molecules. In addition, the uptake of water molecules and their
177 transport due to warming during advection was counteracted by diffusion of water mol-
178 ecules due to the temperature gradient. As thermally induced diffusion was opposite to
179 the airflow gradient, a backflow of water vapor occurred and the two opposite fluxes
180 counteracted each other. The Peclet numbers ($Pe = u_D \cdot d_{\text{mean}}/D$, where D is the diffusion
181 coefficient of water vapor in air), describing the ratio of mass transfer between diffusion
182 and advection, measured during each experiment, showed that diffusion was still domi-
183 nant (Table 1). Therefore, water molecules were diffused along the opposite direction to
184 the temperature gradient and advected along the flow direction leading to a back and
185 forth transport of water molecules.

186 As a Peclet higher than 1 is not possible in snow (Ebner et al., 2015a), advection of
187 cold saturated air into a slightly warmer snowpack has a significant influence not on the
188 total net mass change but on the structural change of the ice grains due to redistribution

189 of water vapour on the ice matrix. Also the increasing pore size has an influence on the
 190 flow field leading to a deceleration of the flow and therefore the interaction of an air-
 191 parcel with the ice matrix in the pores increases due to higher residence time. In addi-
 192 tion, the diffusive transport rises whereas the advective transport decreases changing the
 193 mass transport in the pores. Our results support the hypothesis of Neumann et al. (2009)
 194 that sublimation is limited by vapor diffusion into the pore space rather than sublimation
 195 at crystal faces. This is supported by the temporal evolution of the porosity (Fig. 4 b))
 196 and the SSA (Fig. 4 c)), as no velocity dependence was observed and the structural
 197 changes were too small to be detected by the micro-CT.

198 The influence of diffusion of water vapor in the direction of the temperature gradi-
 199 ent and the influence of the residence time of an air-parcel in the pores were also con-
 200 firmed by a low mass change at the ice-air interface. Overlapping two consecutive 3D
 201 images, the order of magnitude of freshly sublimated ice was detected. The absolute
 202 mass change at the ice-air interface ($\text{kg m}^{-3} \text{ s}^{-1}$) estimated by the experimental results is
 203 defined as

$$204 \quad S_{\text{m,exp}} = \left| \rho_i \frac{\Delta(1-\varepsilon)}{\Delta t} \right| \quad (1)$$

205 where $\Delta(1-\varepsilon)$ is the change in the porosity between two images separated by the time
 206 step Δt , and ρ_i is the density of ice. Albert and McGilvary (1992) and Neumann et al.
 207 (2009) presented a model to calculate sublimation rates directly in an aggregate snow
 208 sample

$$209 \quad S_{\text{m}} = |h_{\text{m}} \text{SA}_{\text{v}} (\rho_{\text{sat}} - \rho_{\text{v}})| \quad (2)$$

210 where SA_{v} is the specific surface area per volume of snow, and h_{m} is the mass-transfer
 211 coefficient (m s^{-1}) given by Neumann et al., (2009)

$$212 \quad h_{\text{m}} = (0.566 \cdot \text{Re} + 0.075) \cdot 10^{-3} \quad (3)$$

213 assuming that the sublimation occurs within the first few mm of the sample. Re ($\text{Re} =$
 214 $u_{\text{D}} \cdot d_{\text{mean}} / \nu$ where ν is the kinematic viscosity of the air) is the corresponding Reynolds-
 215 number of the flow. The absolute sublimation rate is driven by the difference between
 216 the local vapor density (ρ_{v}) and the saturation vapor density (ρ_{sat}) (Neumann et al., 2009;
 217 Thorpe and Mason, 1966). Table 2 shows the estimated absolute sublimation rate by the
 218 experiment (Eq. (1)) and the model (Eq. (2)). The very small change in porosity due to
 219 densification during the first 18 h for ‘ota2’ was not taken into account. The estimated
 220 sublimation rates by the experiment were two orders of magnitude lower than the mod-

221 eled values and also two orders of magnitude lower than during a negative temperature
222 gradient along an airflow experiment (Ebner et al., 2015b). As the air in the pore space
223 is always saturated (Neumann et al., 2009), the back diffusion of water vapor in the op-
224 posite direction of the temperature gradient led to a lower mass transfer rate of sublima-
225 tion. The flow rate dependence for the model described is shown by the mass-transfer
226 coefficient (Eq. 3), increasing with higher airflow. However, the values calculated from
227 the experiment showed a different trend. Increasing the flow rate led to a lower mass
228 transfer rate due to a lower residence time of the air in the pores. Transfer of heat to-
229 ward and water vapor away from the sublimating interface may also limit the sublima-
230 tion rate. In general, the results of the model by Neumann et al. (2009) have to be inter-
231 preted with care, as his model was set up to saturate dry air under isothermal conditions.
232 Ice crystals sublimated as dry air enters the snow sample; water vapor was advected
233 throughout the pore space by airflow until saturation vapor pressure was reached, pre-
234 venting further sublimation. The model by Neumann et al. (2009) does not consider the
235 influence of a temperature gradient and the additional vapor pressure gradient. Howev-
236 er, our results concluded that a positive temperature gradient along the airflow has a
237 significant impact on the sublimation rate decreasing the rate by two orders of magni-
238 tude.

239 In the experiments by Neumann et al. (2009), sublimation of snow using dry air un-
240 der isothermal condition showed a temperature drop for approximately the first 15 min
241 after sublimation started and stayed constant because the latent heat absorption of sub-
242 limation for a given flow rate and heat exchange with the sample chamber equalized
243 each other. Such a temperature drop was not observed in our experiments. In the exper-
244 iments by Neumann et al. (2009) the amount of energy used for sublimation was be-
245 tween -10 and -40 J min^{-1} for saturation of dry air. Using the expected mass change at
246 the ice-air interface $S_{m,\text{exp}}$ (Eq. (1)) and the latent heat of sublimation ($L_{\text{sub}} \approx 2834.1 \cdot$
247 10^3 J kg^{-1}) the energy needed for sublimation ranged between -2 and -12 J min^{-1} for our
248 experiments. Our estimated values are a factor up to five lower than the estimated num-
249 bers of Neumann et al. (2009), because the entering air was already saturated (with ref-
250 erence to the cold temperature) at the inlet. The needed energy for sublimation could be
251 balanced between the sensible heat carried into and out of the sample, and the exchange
252 of the snow sample with the air stream and the surrounding prevented a temperature
253 drop.

254 Thermal conductivity changed insignificantly in these experiments, especially for
255 ‘ota 1’. This indicates that air warming by a positive temperature gradient along the air-
256 flow and an open system reduces or suppresses the increase in thermal conductivity
257 usually observed by temperature gradient metamorphism (Loewe et al., 2013; Calonne
258 et al., 2014). Compared to closed temperature gradient experiment, the applied tempera-
259 ture gradient and the open system induced an air movement and therefore reduced the
260 impact on the thermal conductivity, at least on the short term.

261

262 **6. Summary and conclusion**

263 We performed four experiments of temperature-gradient metamorphism of snow
264 under saturated advective airflow during 108 h. Cold saturated air was blown into the
265 snow samples and warmed up while flowing across the sample. The temperature gradi-
266 ent varied between 43 and 53 K m⁻¹ and the snow microstructure was observed by X-ray
267 micro-tomography every 3 h. The micro-CT scans were segmented, and porosity, spe-
268 cific surface area, and the mean pore-size were calculated. Effective thermal conductivi-
269 ty was calculated in direct pore-level simulations (DPLS).

270 Compared to deposition (shown in Ebner et al., 2015b), sublimation showed a small
271 effect on the structural change of the ice matrix. A change in the pore size was most
272 likely due to sublimation of ice crystals with small radii but a significant loss of water
273 molecules of the snow sample and mass transfer away from the ice interface due to sub-
274 limation and advective transport could not be detected by the micro-CT scans and no
275 flow rate dependence was observed. The interaction of mass transport of advection and
276 diffusion of water vapor in the opposite direction of the temperature gradient and the
277 influence of the residence time of an air-parcel in the pores led to a negligible total mass
278 change of the ice. However, a strong reposition of water molecules on the ice grains was
279 observed.

280 The energy needed for sublimation was too low to see a significant temperature drop
281 because the needed energy was balanced between the sensible heat carried into and out
282 of the sample, and the exchange of the snow sample with the air stream and the sur-
283 rounding.

284 This is the third paper of a series analyzing an advective airflow in a snowpack in
285 depth of more than 1 cm. Previous work showed that: (1) under isothermal conditions,

286 the Kelvin-effect leads to a saturation of the pore space in the snow but did not affect
287 the structural change (Ebner et al., 2015a); (2) applying a negative temperature gradient
288 along the flow direction leads to a change in the microstructure and creation of whisker-
289 like structures due to deposition of water molecules on the ice matrix (Ebner et al.,
290 2015b); and (3) a positive temperature gradient along to the flow had a negligible total
291 mass change of the ice but a strong reposition effect of water molecules on the ice
292 grains, shown in this paper. Conditions (1) and (3) showed that they have a negligible
293 effect on the porosity evolution of the ice matrix. Porosity changes can be neglected to
294 improve models for snow compaction and evolution at the surface. In contrast, condi-
295 tions (2) showed a significant impact on the structural evolution and seems to be essen-
296 tial for such snowpack models and other numerical simulations. Nevertheless, the strong
297 reposition of water molecules on the ice grains observed for all conditions (1) – (3) can
298 have a significant impact on atmospheric chemistry and isotopic changes in snow.

299

300 **Acknowledgements**

301 The Swiss National Science Foundation granted financial support under project Nr.
302 200020-146540. The authors thank the reviewers E. A. Podolskiy and F. Flin for the
303 constructive reviews and M. Jaggi, S. Grimm, H. Löwe for technical and modelling
304 support.

305

306 **References**

- 307 Albert, M. R.: Effects of snow and firn ventilation on sublimation rates, *Annals of Glac-*
308 *iology*, 35, 52-56, 2002.
- 309 Albert, M. R. and Hardy, J. P.: Ventilation experiments in a seasonal snow cover, in *Bi-*
310 *ogeochemistry of Seasonally Snow-Covered Catchments*, IAHS Publ. 228, edited
311 by K. A. Tonnessen, M. W. Williams, and M. Tranter, 41 –49, IAHS Press, Wall-
312 ington, UK, 1995.
- 313 Albert, M. R. and McGilvary, W. R.: Thermal effects due to air flow and vapor
314 transport in dry snow, *Journal of Glaciology*, 38, 273-281, 1992.
- 315 Box, J. E. and Steffen, K.: Sublimation on the Greenland ice sheet from automated
316 weather station observations, *Journal of Geophysical Research*, 107, 33965-33981,
317 2001.

318 Calonne, N, Flin, F., Morin, S., Lesaffre, B., and Rolland du Roscoat, S.: Numerical and
319 experimental investigations of the effective thermal conductivity of snow, *Geo-*
320 *physical Research Letter*, 38, 1-6, 2011.

321 Calonne, N., Geindreau, C., Flin, F., Morin, S., Lesaffre, B., Rolland du Roscoat, S.,
322 and Charrier, P.: 3-D image-based numerical computations of snow permeability:
323 links to specific surface area, density, and microstructural anisotropy, *The Cry-*
324 *osphere*, 6, 939-951, 2012.

325 Calonne, N., Flin, F., Geindreau, C., Lesaffre, B. and Rolland du Roscoat, S.: Study of a
326 temperature gradient metamorphism of snow from 3-D images: time evolution of
327 microstructures, physical properties and their associated anisotropy, *The Cry-*
328 *osphere*, 8, 2255-2274, 2014.

329 Chen, S., and Baker, I.: Evolution of individual snowflakes during metamorphism,
330 *Journal of Geophysical Research*, 115, 1–9, 2010.

331 Colbeck, S. C.: Air movement in snow due to windpumping, *Journal of Glaciology*, 35,
332 209–213, 1989.

333 Déry, S. J. and Yau, M. K.: Large-scale mass balance effects of blowing snow and sur-
334 face sublimation, *Journal of Geophysical Research*, 107,
335 doi:10.1029/2001JD001251, 2002.

336 Ebner, P. P., Grimm, S., Schneebeli, M., and Steinfeld, A.: An instrumented sample
337 holder for time-lapse micro-tomography measurements of snow under advective
338 conditions, *Geoscientific Instrumentation Methods and Data Systems*, 3, 179–185,
339 2014.

340 Ebner, P. P, Schneebeli, M., and Steinfeld, A.: Tomography-based observation of iso-
341 thermal snow metamorphism under advective conditions, *The Cryosphere*, 9, 1363–
342 1371, 2015a.

343 Ebner, P. P, Andreoli, C., Schneebeli, M., and Steinfeld, A.: Tomography-based obser-
344 vation of ice-air interface dynamics of temperature gradient snow metamorphism
345 under advective conditions, *Journal of Geophysical Research*, submitted, 2015b.

346 Ekaykin, A. A., Hondoh, T., Lipenkov, V. Y., and A. Miyamoto: Post-depositional
347 changes in snow isotope content: preliminary results of laboratory experiments,
348 *Clim. Past Discuss.*, 5, 2239–2267, 2009.

349 Gjessing, Y. T.: The filtering effect of snow, in: *Isotopes and Impurities in Snow and*
350 *Ice Symposium*, edited by: Oeschger, H., Ambach, W., Junge, C. E., Lorius, C., and
351 Serebryanny, L., 118, IASH-AISH Publication, Dorking, 199–203, 1977.

352 Haussener, S., Gergely, M., Schneebeli, M., and Steinfeld, A.: Determination of the
353 macroscopic optical properties of snow based on exact morphology and direct pore-
354 level heat transfer modeling, *Journal of Geophysical Research*, 117, 1–20, 2012.

355 Kaempfer, T. U., Schneebeli, M. and Sokratov, S. A.: A microstructural approach to
356 model heat transfer in snow, *Geophysical Research Letter*, 32, 1-5, 2005.

357 Kaempfer, T. U. and Plapp, M.: Phase-field modeling of dry snow metamorphism,
358 *Physical Review E*, 79, <http://dx.doi.org/10.1103/PhysRevE.79.031502>, 2009.

359 Löwe, H., Spiegel, J. K., and Schneebeli, M.: Interfacial and structural relaxations of
360 snow under isothermal conditions, *Journal of Glaciology*, 57, 499–510, 2011.

361 Löwe, H., Riche, F., and Schneebeli, M.: A general treatment of snow microstructure
362 exemplified by an improved relation for the thermal conductivity, *The Cryosphere*
363 *Discussions*, 6, 4673–4693, (2012).

364 Neumann, T. A., Albert, M. R., Lomonaco, R., Engel, C., Courville, Z., and Perron, F.:
365 Experimental determination of snow sublimation rate and stable-isotopic exchange,
366 *Annals of Glaciology*, 49, 1–6, 2008

367 Neumann, T. A., Albert, M. R., Engel, C., Courville, Z., and Perron, F.: Sublimation
368 rate and the mass-transfer coefficient for snow sublimation, 52, 309-315, 2009.

369 Otsu, N.: A Threshold Selection Method from Gray-Level Histograms, *IEEE Transac-*
370 *tions on Systems Man and Cybernetics*, 9, 62–66, 1979.

371 Petrasch, J., Schrader, B., Wyss, P., and Steinfeld, A.: Tomography-based determination
372 of effective thermal conductivity of fluid-saturated reticulate porous ceramics,
373 *Journal of Heat Transfer*, 130, 1-10, 2008.

374 Pinzer, B. R., and Schneebeli, M.: Snow metamorphism under alternating temperature
375 gradients: Morphology and recrystallization in surface snow, *Geophysical Research*
376 *Letters*, 36, 1–4, 2009.

377 Pinzer, B. R., Schneebeli, M., and Kaempfer, T. U.: Vapor flux and recrystallization
378 during dry snow metamorphism under a steady temperature gradient as observed by
379 time-lapse micro-tomography, *The Cryosphere*, 6, 1141–1155, 2012.

380 Riche, F. and Schneebeli, M.: Thermal conductivity of snow measured by three inde-
381 pendent methods and anisotropy considerations, *The Cryosphere*, 7, 217–227,
382 (2013).

383 Schleef, S., Jaggi, M., Löwe, H., and Schneebeli, M.: Instruments and Methods: An im-
384 proved machine to produce nature-identical snow in the laboratory, *Journal of Glac-*
385 *iology*, 60, 94–102, 2014.

386 Stichler, W., Schotterer, U., Frohlich, K., Ginot, P., Kull, C., Gäggeler, H., and
387 Pouyaud, P.: Influence of sublimation on stable isotope records recovered from
388 high-altitude glaciers in the tropical Andes, *Journal of Geophysical Research*, 106,
389 22613-22630, 2001.

390 Sturm, M. and Benson, C.: Vapor transport grain and depth-hoar development in the
391 subarctic snow, *Journal of Glaciology*, 43, 42-59, 1997.

392 Sturm, M., and Johnson, J. B.: Natural convection in the subarctic snow cover, *Journal*
393 *of Geophysical Research*, 96, 11657–11671, 1991.

394 Thorpe, A. D. and Mason, B. J.: The evaporation of ice spheres and ice crystals, *British*
395 *Journal of Applied Physics*, 17, 541-548, 1966.

396 Waddington, E. D., Cunningham, J., and Harder, S. L.: The effects of snow ventilation
397 on chemical concentrations, in: *Chemical Exchange Between the Atmosphere and*
398 *Polar Snow*, edited by: Wolff, E. W. and Bales, R. C., NATO ASI Series, 43,
399 Springer, Berlin, 403–452, 1996.

400 Wang, X. and Baker, I.: Evolution of the specific surface area of snow during high-
401 temperature gradient metamorphism, *Journal of Geophysical Research Atmos-*
402 *phere.*, 119, 13690–13703, 2014

403 Zermatten, E., M. Schneebeli, H. Arakawa, and A. Steinfeld: Tomography-based deter-
404 mination of porosity, specific area and permeability of snow and comparison with
405 measurements, *Cold Regions Science and Technology*, 97, 33–40, 2014,
406 doi:10.1016/j.coldregions.2013.09.013.

407

408

409 **Table 1:** Morphological and flow characteristics of the experiments: Volume flow (\dot{V}),
 410 initial superficial velocity in snow ($u_{D,0}$), initial snow density (ρ_0), initial porosity (ε_0),
 411 specific surface area (SSA_0), initial mean pore size (d_{mean}), average inlet ($T_{\text{in,ave}}$) and
 412 outlet temperature ($T_{\text{out,ave}}$), and the average temperature gradient (∇T_{ave}), corresponding
 413 Reynolds number (Re) and Peclet number (Pe).

414

Name	\dot{V} liter min ⁻¹	$u_{D,0}$ m s ⁻¹	ρ_0 kg m ⁻³	ε_0 –	SSA_0 m ² kg ⁻¹	d_{mean} mm	$T_{\text{in,ave}}$ °C	$T_{\text{out,ave}}$ °C	∇T_{ave} K m ⁻¹	Re –	Pe –
ota1	–	–	284.3	0.69	25.0	0.30	-13.8	-12.5	43.3	–	–
ota2	0.3	0.004	256.8	0.72	26.3	0.33	-14.0	-12.5	50.0	0.07	0.05
ota3	1.0	0.012	256.8	0.72	24.3	0.34	-13.8	-12.3	43.3	0.25	0.19
ota4	3.0	0.036	265.9	0.71	21.7	0.36	-14.6	-13.0	53.3	0.78	0.61

415

416

417

418 **Table 2:** Estimated sublimation rate S_m using the mass transfer coefficient h_m deter-
 419 mined by Neumann et al. (2009) and the corresponding average surface area per volume
 420 $SA_{V,\text{ave}}$. S_m can be compared with the measured sublimation rate of the experiment $S_{m,\text{exp}}$
 421 (Eq. (1)).

422

Name	$SA_{V,\text{ave}}$ mm ⁻¹	h_m m s ⁻¹	S_m kg m ⁻³ s ⁻¹	$S_{m,\text{exp}}$ kg m ⁻³ s ⁻¹
ota1	22.44	$0.75 \cdot 10^{-4}$	$4.83 \cdot 10^{-4}$	$0.68 \cdot 10^{-6}$
ota2	23.98	$1.15 \cdot 10^{-4}$	$2.99 \cdot 10^{-4}$	$4.48 \cdot 10^{-6}$
ota3	21.88	$2.17 \cdot 10^{-4}$	$5.15 \cdot 10^{-4}$	$0.76 \cdot 10^{-6}$
ota4	19.61	$5.16 \cdot 10^{-4}$	$10.9 \cdot 10^{-4}$	$0.08 \cdot 10^{-6}$

423

424 **Figure captions**

425 **Fig. 1.** Schematic of the ice-air interface transport processes: a) Under isothermal
426 conditions Kelvin-effect leads to a saturation of the pore space in the snow
427 but did not affect the structural change (Ebner et al., 2015a); b) Air cooling
428 by a negative temperature gradient along the flow direction leads to a
429 change in the microstructure due to deposition (Ebner et al., 2015b); c) Air
430 warming by a positive temperature gradient along the flow has a negligible
431 total mass change of the ice but a strong reposition effect of water molecules
432 on the ice grains, shown in this paper.

433 **Fig. 2.** Evolution of the 3-D structure of the ice matrix with applied temperature
434 gradient and advective conditions. Experimental conditions (from left to
435 right) at different measurement times from beginning to the end (top to bot-
436 tom) of the experiment. The shown cubes are $110 \times 40 \times 110$ voxels ($2 \times$
437 0.7×2 mm³) large with 18 μ m voxel size (a high resolution figure can be
438 found in supplementary material).

439 **Fig. 3.** Superposition of vertical cross-section parallel to the flow direction at time
440 0 and 108 hours for ‘ota3’ (left panel) and ‘ota4’ (right panel). Sublimation
441 and deposition of water vapor on the ice grains were visible with an uncer-
442 tainty of 6 % (a high resolution figure can be found in supplementary mate-
443 rial).

444 **Fig. 4.** Temporal evolution of a) the mean pore size, d_{mean} , of the snow samples ob-
445 tained by an opening-size distribution, b) the porosity, ε , obtained by trian-
446 gulated structure surface method, c) the specific surface area, SSA, of the
447 ice matrix obtained by triangulated structure surface method, and d) the ef-
448 fective thermal conductivity of the snow sample, k_{cond} , estimated by DPLS
449 simulations. The sizes of the volumes used for the computation of each
450 property are $350 \times 350 \times 350$ voxels ($6.3 \times 6.3 \times 6.3$ mm³).

451

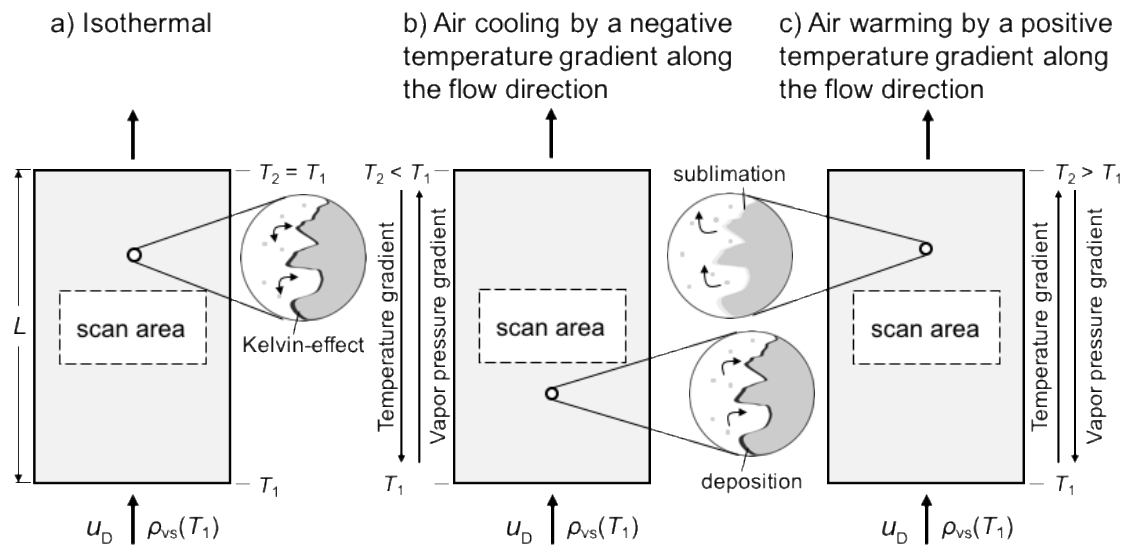


Fig. 1

452

453

454

455

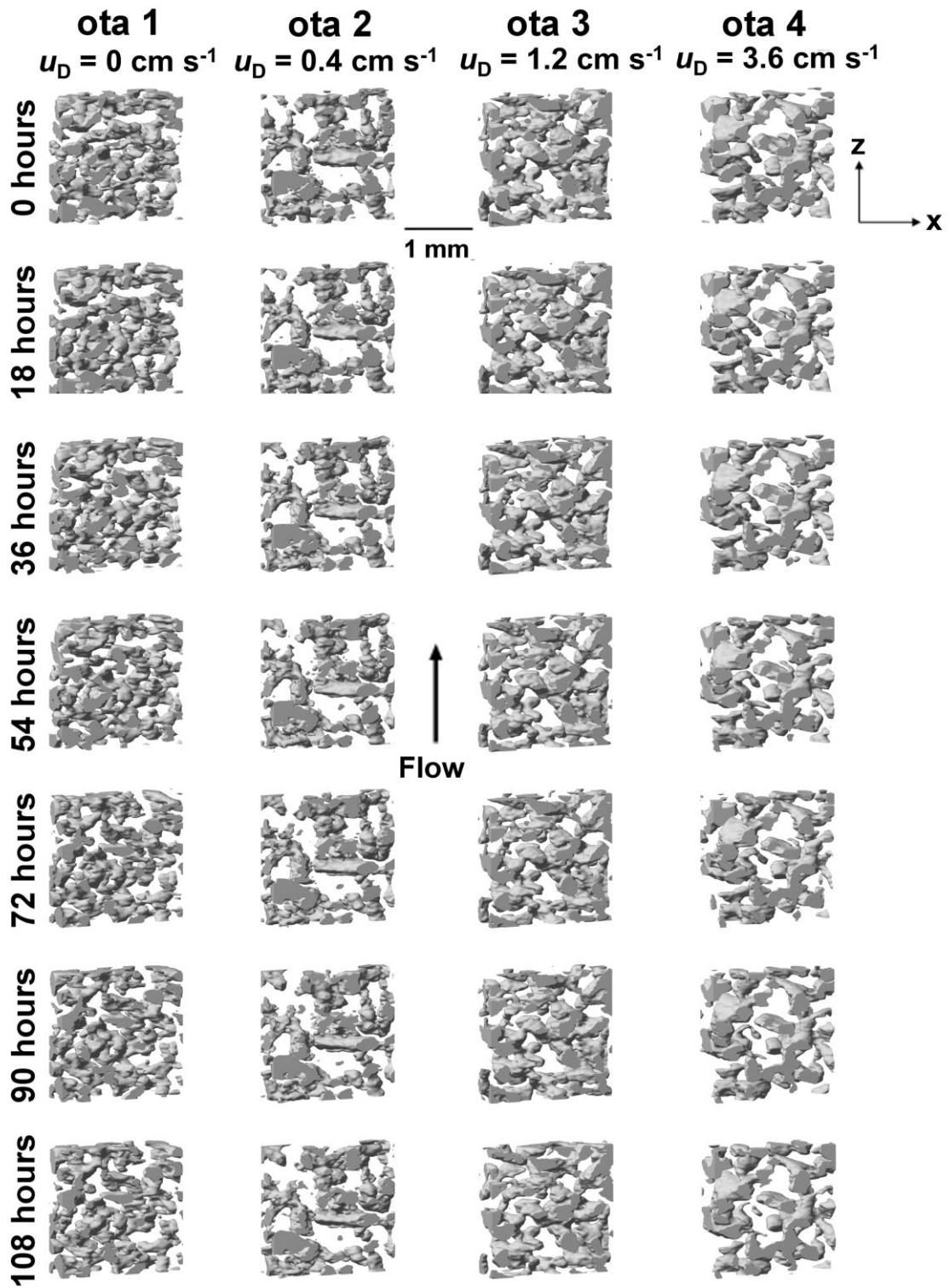


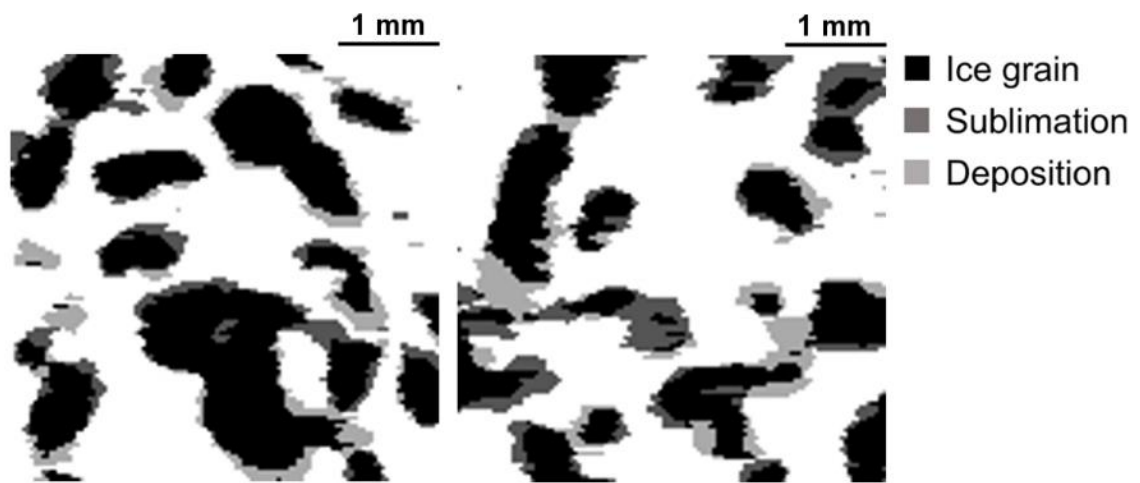
Fig. 2

456

457

458

459



460

461

462

Fig. 3

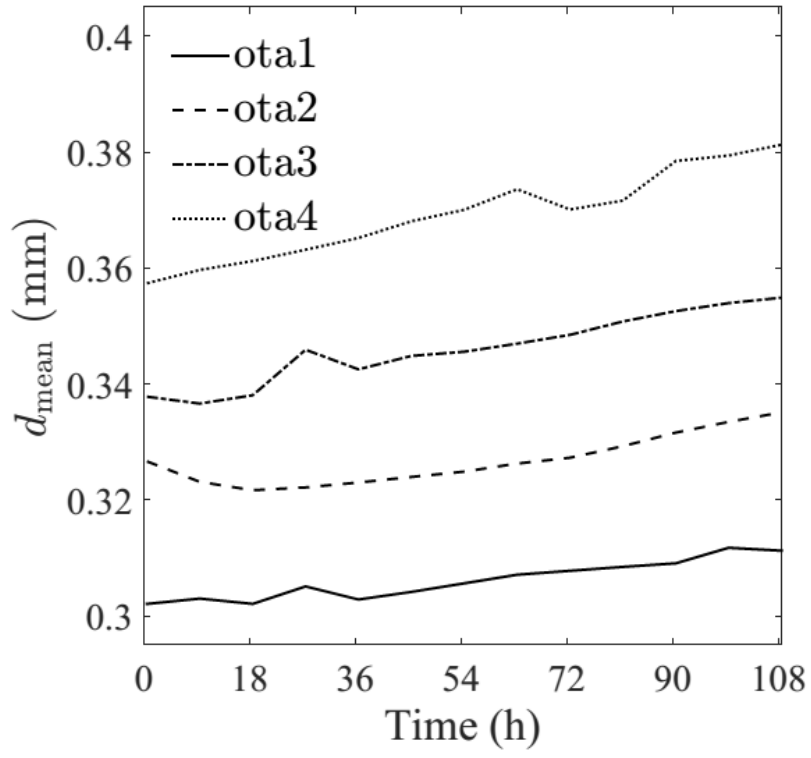


Fig. 4 a)

463

464

465

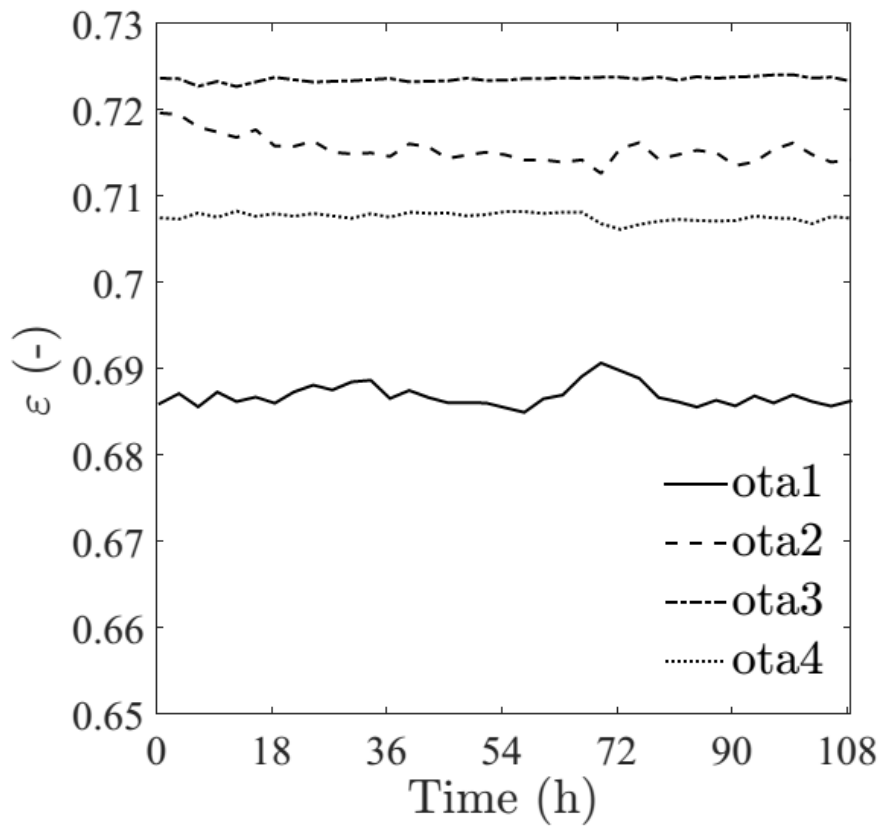


Fig. 4 b)

466

467

468

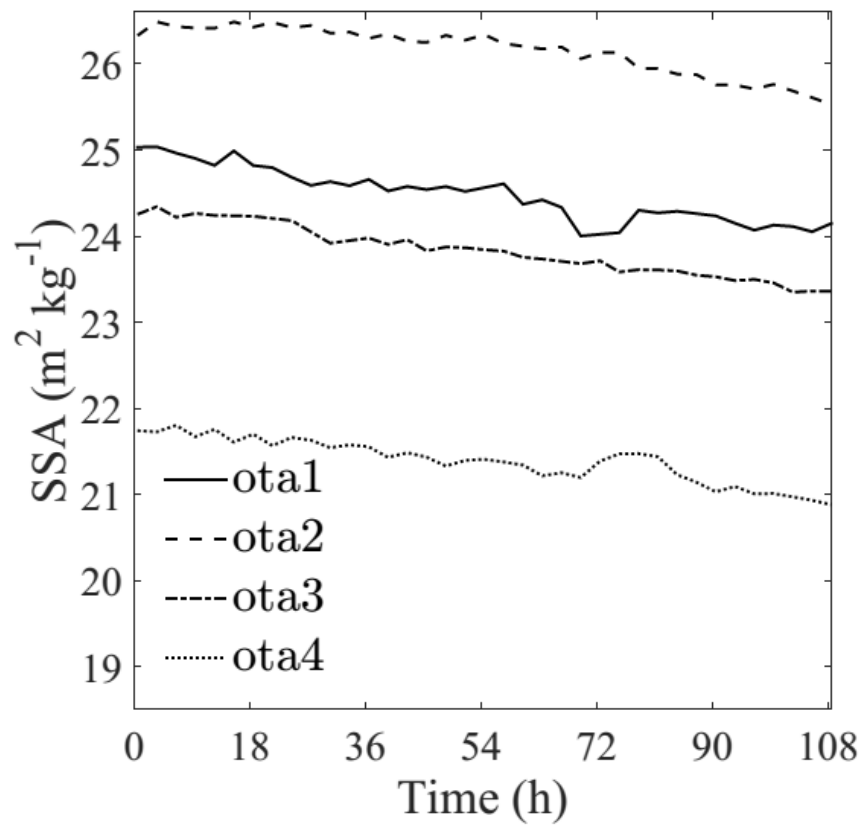
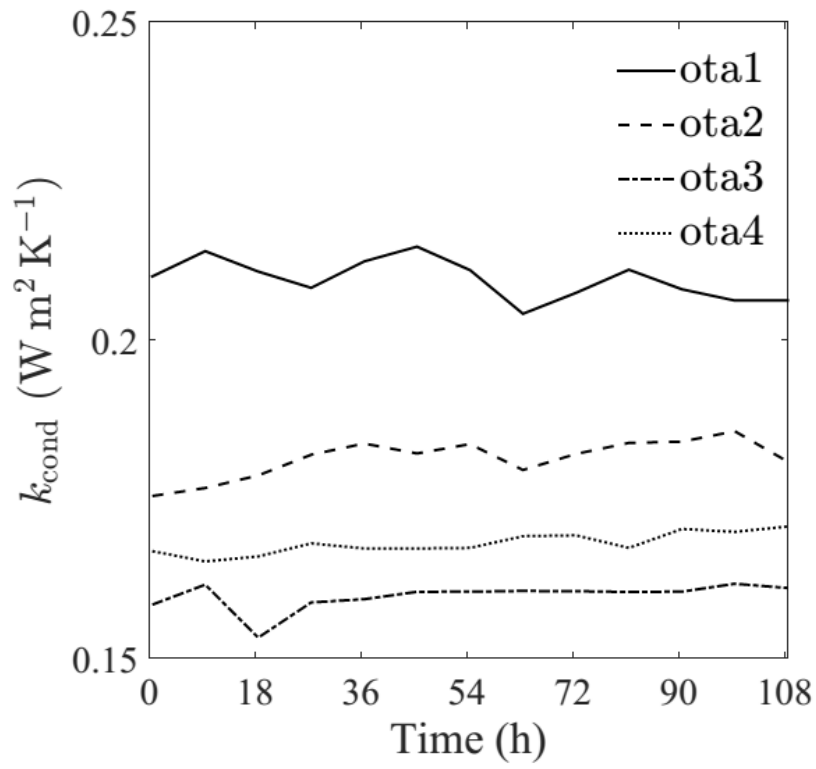


Fig. 4 c)

469

470

471



472

473

Fig. 4 d)